Vol. 20, No. 2 (2021) 787-805
Revista Mexicana de Ingeniería Química

Surface roughness and textural image analysis, particle size and stability of microparticles obtained by microfluidization of soy protein isolate aggregates suspensions

Rugosidad superficial y análisis de imágenes textural, tamaño de partícula y estabilidad de micropartículas obtenidas por microfluidización de suspensiones de agregados de aislado de proteína de soya

I. Monroy-Rodríguez[1], G. F. Gutiérrez-López[1*], H. Hernández-Sánchez[1], R. E. López-Hernández[1], M. Cornejo-Mazón[2], L. Dorántes-Álvarez[1], L. Alamilla-Beltrán[1]

[1]*Instituto Politécnico Nacional, Escuela Nacional de Ciencias Biológicas, Departamento de Ingeniería Bioquímica. Carpio y Plan de Ayala S/N, Santo Tomás 11340, Ciudad de México.*
[2]*Instituto Politécnico Nacional, Escuela Nacional de Ciencias Biológicas, Departamento de Biofísica. Carpio y Plan de Ayala S/N, Santo Tomás 11340, Ciudad de México.*

Received: December 20, 2020; Accepted: February 4, 2021

Abstract

Protein microparticles are of interest in the development of low-fat foods and as stabilizing agents of food dispersed systems. The characteristics of the microparticles influence food texture, so that it is important to consider the processing conditions for their production. In this work, soy protein isolate (SPI) aggregates obtained by heat treatment (93 °C for 15 min) and different pH values (3, 5, 7 and 9) were subjected to microfluidization (110 MPa, 1, 2 or 3 cycles). The resulting SPI suspensions were evaluated for particle size, zeta potential and Turbiscan stability index (TSI). The TSI of SPI microparticles suspensions (TSI) was better at pH 9 (and 1 MF cycle) due to the distance from the average isoelectric point for soy proteins (4.5). By atomic force microscopy it was possible to observe the breakdown of the aggregates. In all cases, a decrease in height's profiles was observed after MF, which confirmed the reduction in particle size of the microparticles. Surface roughness and image texture analyses allowed to evaluate the effect of MF on the surface of the microparticles. The best descriptor of the image texture characteristics of microparticles was the second angular moment while the rest of the descriptors did not correlate with the characteristics of the images in the whole range of operating conditions given that their calculation algorithms were not sensitive enough to detect the small variations in image texture of the samples.

Keywords: microfluidization, soy protein isolate, microparticles stability, texture image analysis.

Resumen

Las micropartículas de proteínas son de interés en el desarrollo de alimentos bajos en grasas y como agentes estabilizantes en de sistemas dispersos en alimentos. Las características de las micropartículas influyen en la textura de los alimentos, por lo que es importante considerar las condiciones de procesamiento para su producción. En este trabajo, agregados de aislados de proteína de soya (SPI) obtenidos por tratamiento térmico (93 °C durante 15 min) y diferentes valores de pH (3, 5, 7 y 9) fueron sometidos a microfluidización (MF) (110 MPa, 1, 2 o 3 ciclos). Las suspensiones resultantes se evaluaron en cuanto al tamaño de partícula, potencial zeta y el índice de estabilidad de Turbiscan (TSI). La estabilidad de la suspensión de micropartículas SPI fue mejor a pH 9 (y 1 ciclo de MF) debido a la distancia del punto isoeléctrico promedio para las proteínas de soja (4.5). Por microscopía de fuerza atómica (AFM) fue posible observar la ruptura de los agregados. En todos los casos, se observó una disminución en los perfiles de altura después de la MF, lo que confirmó la reducción del tamaño de partícula de las micropartículas. Los análisis de rugosidad superficial y textura de imagen permitieron evaluar el efecto de la MF en la superficie de las micropartículas. El descriptor más relevante para la caracterización de micropartículas fue el segundo momento angular mientras que el resto de los descriptores no se correlacionaron con las características de las imágenes en todo el intervalo de condiciones de operación dado que sus algoritmos de cálculo no fueron lo suficientemente sensibles para detectar las pequeñas variaciones en la rugosidad de las muestras.

Palabras clave: microfluidización, aislado de proteína de soya, estabilidad de micropartículas, análisis de textura de imágenes.

* *Corresponding author. E-mail*: gusfgl@gmail.com
https://doi.org/10.24275/rmiq/Alim2311
ISSN:1665-2738, *issn-e*: 2395-8472

1 Introduction

Microfluidization (MF) also known as Dynamic High-Pressure Microfluidization (DHPM) is a homogenization process in which mechanical energy is transferred to fluid particles under high dynamic pressures (Pereyra-Castro *et al*., 2019; Liu *et al*., 2016; Cano-Sarmiento *et al*., 2015; Kasaai *et al*., 2003). The homogenization system of MF consists of a pump that drives the dispersion through microchannels within the disruption or interaction chamber (IXC) (Villalobos-Espinosa *et al*., 2019; Cano-Sarmiento *et al*., 2015). MF is of interest in food engineering due to produced changes in structure and functionality in polymers as polysaccharides and proteins (Monroy-Rodríguez *et al.,* 2020; Monroy-Villagrana *et al*., 2014).

MF can change the structure of proteins, inducing unfolding of the protein and influencing their physicochemical properties (Liu *et al.,* 2010). Some of the proteins in which the effect of MF has been evaluated are those from peanut (Hu *et al.,* 2011, Gong *et al.,* 2017, Gong *et al*., 2019), milk whey (Liu *et al.,* 2011), β-lactoglobulin (Zhong *et al.,* 2012), soy (Song *et al.,* 2013; Shen and Tang, 2012; Martínez *et al.,* 2011; Keerati-U-Rai and Corredig, 2009) and zein (Sun *et al.,* 2016) among others. Microparticles are produced by the aggregation of the proteins by pH or heat, and subsequent mechanical treatment as MF causing a rather homogeneous reduction in particle size.

There are published reports of the various effects of MF in proteins but the combination of a high temperature and pH, has not been widely studied in spite of their importance in the production of protein microparticles, used in processed foods as fat substitute (Chung *et al.,* 2014). It is believed that the application of microfluidization cycles and different pH values and a fixed high temperature of the suspensions would produce microparticles with different levels of stability and morphometry. The functionality of microparticles in food emulsions is comparable to that imparted by the oil droplets, whose particle sizes and morphology may contribute to enhance the textural properties of food systems, by altering the local relative motion of the dispersed phase (Liu *et al*., 2016; Torres *et al.,* 2011). The range of particle sizes of microparticles is between 0.1 and 10 μm (Torres *et al.,* 2011).

Milk whey proteins are widely used for the formation of microparticles by MF (Madadlou *et al.,* 2018; Ipsen 2017; Chung *et al.,* 2014; Dissanayake *et al.,* 2010; Iordache and Jelen, 2003; Laneuville *et al.,* 2000) whereas, microparticles of vegetable proteins have received less attention despite their importance for developing plant-based protein foods (Ipsen, 2017). Liu and Tang (2013) obtained soy protein aggregates by combining heat treatment and ionic strength handling (using NaCl) at neutral pH, obtaining particles with an average size of 100 nm, used for the stabilization of Pickering emulsions processed by MF.

In this work, the effect of MF on the formation of soy protein microparticles was analyzed given that this protein is highly marketable and common to find in processed foods due to technological functionalities and nutritional value. The aim of the present work was to obtain SPI aggregates by combined heat (93°C, 15 min) and different pH (3, 5, 7 and 9) treatments, and evaluate the effect of applying MF (110 MPa, 1, 2 or 3 cycles) on the surface roughness and textural image analysis, particle size and suspension stability of the SPI microparticles.

2 Materials and methods

2.1 Preparation of SPI suspensions

Soy protein isolate (SPI) (ProWinner®, Mexico City, Mexico) suspensions in deionized water 3% (w/v) were prepared and their pH were adjusted to 3, 5, 7 and 9 by using either 1 M HCl (Sigma-Aldrich) or 1 M NaOH (Sigma-Aldrich) (Acosta-Dominguez *et al.,* 2016). This concentration of protein was selected based on published reports (Gong *et al*., 2017 and 2019; Sun *et al*., 2016; Song *et al*., 2013; Hu *et al.,* 2011) indicating that a 1-7% concentration range of protein is recommended to avoid clogging of the microchannels of the microfluidizer. To inhibit microbial growth in the samples, sodium azide (Sigma-Aldrich) (0.02% w/v) was added to the suspensions (Liu and Tang, 2013). The protein content of the isolate was confirmed by Kjeldahl analysis (AOAC 2.062, 1984) obtaining a protein content of 87.15% ± 0.16. The equipment used to carry out this analysis was a Kjeltec™ 8100 Manual Distillation Unit, Foss™, Canada. The chemical used (H_2SO_4, Wesselow indicator, NaOH, H_3BO_4, HCl were purchased from Sigma-Aldrich).

2.2 Microparticulation process

For the preparation of protein aggregates, the suspensions prepared as described above were heated for 15 min in a water bath at 93 °C as recommended by various authors (Chen *et al.,* 2017; Liu and Tang, 2013; Shen and Tang, 2012) who reported that the highest concentration of aggregates occurred at temperatures above 90 °C during at least 15 min in such a way that by maintaining the temperature fixed at 93°C, it would be possible to observe the effect of the pH and the number of cycles during the preparation of microparticles while warranting formation of aggregates. Subsequently, the suspensions were subjected to MF in a Microfluidizer® equipment (LM10, Microfluidics International Corporation, England) at 110 MPa; samples were collected after 1, 2 and 3 MF cycles (Monroy-Villagrana *et al*., 2014).

2.3 Particle size (PS) and polydispersity index (PDI) measurements

The PS and PDI of microparticles were evaluated by using a Zetasizer Nano Zs (Nano Zs, Malvern Panalytical, Malvern, England). All measurements were carried out in 1:1000 (v/v) suspensions (Bernewitz *et al*., 2011) and determinations were carried out by triplicate. Particle sizes were evaluated by using dynamic light scattering (DLS), which is a well-established and non-invasive technique for measuring the size and size distribution of molecules and particles dissolved in liquid. The motion of the particles or molecules in suspension causes the laser light to be scattered at different intensities. From the analysis of the intensity fluctuations, the speed of the particle's motion and therefore their size are obtained by using the Stokes-Einstein equation (Malvern Panalytical, 2021). The software of the equipment ZetaSizer Software 7.12 (Malvern Instruments Ltd, 2016) yields a particle size distribution from which, the PDI values were obtained.

2.4 Zeta potential measurement

The microparticles in suspension were diluted (1:1000 v/v) and the zeta potential (ζ-P) was measured with a Zetasizer Nano Zs (Malvern Instrument, England) (Monroy-Villagrana *et al.,* 2014). All measurements were carried out by triplicate.

2.5 Determination of the Turbiscan Stability Index (TSI) of SPI microparticles suspensions

The stability of the SPI suspensions was analyzed with a Turbiscan^{LAB} meter (Formulation Smart Scientific Analysis, Tolouse, France). This equipment determinates the changes in static multiple light scattering (SMLS) of the sample over time by sending photons (NIR light source, 880nm) to the sample as to determine the scattering profiles of the sample which will change depending on sedimentation due to all phenomena that will cause destabilization of the suspension (Formulation Smart Scientific Analysis, 2021).

The TSI values were taken as indicators of their stability and were obtained by means of Eq. (1) through the software of the equipment (Pereyra-Castro *et al*., 2019; Villalobos-Espinosa *et al*., 2019).

$$TSI = \sqrt{\frac{\Sigma_{i=1}^{n}(X_i - X_{BS})^2}{n-1}} \quad (1)$$

In which:

X_i: is the average backscatter for each minute of the measurement.

X_{BS}: is the mean of X_i values and n is the number of scans.

Higher differences (X_i - X_{BS}) in backscattering readings with time will indicate decreased stability thus larger TSI of the sample and vice versa as given in Equation 1.

2.6 Atomic force microscopy and surface roughness analysis

The samples were diluted (1:1000 v/v) in deionized water and 10 μL were deposited on a glass slide and dried at room temperature. The surface topography of the micro- and nano- soy protein microparticles was analyzed by atomic force microscopy (AFM) (Veeco, diMul-timode V, USA) connected to a diNanoscope V microcontroller, USA by applying the *tapping* mode (Acosta-Domínguez *et al.,* 2016; Alvarado-González *et al*., 2012).

The surface roughness values Ra (arithmetic mean roughness), Rq (mean square roughness) and heights of profiles were obtained from the AFM images by using the Nanoscope Analysis software (version 2.0, Bruker corporation, USA). The scanning area was 5x5μm and Ra and Rq were obtained in the first channel (height) as reported by Acosta-Dominguez *et al*. (2016).

2.7 Texture image analysis

Images of the SPI microparticles (521 × 521 pixels) were captured by using the above described AFM connected to a diNanoscope V microcontroller, USA. Captured images were stored as bitmaps in a gray scale with brightness values between 0 and 255 for each pixel constituting the image (Hernández-Carrion *et al.,* 2015). A generalization of the box counting method was used to evaluate the texture fractal dimension of the images (FDt) (Quintanilla-Carvajal *et al*., 2011). In this work, the shifting differential box-counting method (SDBC) (Chen *et al.,* 2001) was utilized to evaluate the fractal dimension of texture of AFM images by means of the ImageJ software (Rasband, W.S., ImageJ v.1.52 k, National Institutes of Health, Bethesda, Maryland, USA).

Also, the following textural parameters were evaluated to assess their suitability for describing the image texture of the agglomerates from the AFM images: angular second moment, contrast, correlation, inverse difference moment, and entropy. Measurements were carried out by using the Gray-Level Co-Occurrence Matrix (GLCM) plugin and surface plot tools of the ImageJ software as recommended by Hernández-Carrion *et al*. (2015). The GLCM is a typical method for evaluating the texture of images based on spatial-dependence GLCM of pixels with estimation of image features using second-order statistics (Sivchenko *et al*., 2016).

2.8 Statistical analysis

Statistical analyses were carried out by means of an analysis of variance (ANOVA) by applying a significance level $\alpha = 0.05$. All calculations were carried out by using MinitabR 17.1.0 (Minitab Inc., 2013) software and results were expressed as mean values ± standard deviation.

3 Results and discussion

3.1 Particle size (PS) and polydispersity index (PDI)

The particle size and PDI for the suspensions of microparticles are shown in Table 1. The size of the protein aggregates decreased as the number of MF cycles increased, independently of the pH used to form the SPI aggregates. This was indicative that the number of MF cycles did not induce reaggregation of small particles into larger ones due to excess input of energy caused by the application of cycles or pressure over a threshold value (Villalobos-Castillejos *et al.,* 2018). The largest particle sizes were found at pH 5, which is close to the isoelectric point (IP) of the proteins of the SPI (4.5) where an increase in protein aggregation was expected due to the charge balance of the amino acids is close to zero and the interaction with water molecules decreased, which provoked a decrement in protein solubility at this pH (González-Cruz *et al.,* 2020; Achouri *et al.,* 2005). When the pH of the suspensions was increased to 7 and 9 (far from the IP of SPI), MF decreased significantly ($p \leq 0.05$) the particle size, and the lowest particle sizes and PDI were obtained at pH 9 and when 3 MF cycles were used. At pH 9, SPI solubility increased, and enough energy was supplied for disrupting non-covalent bonds such as hydrogen, hydrophobic, hydrophilic and electrostatic interactions in the protein chains, aggregates and networking structures (Song *et al.,* 2013; Tang *et al.,* 2009) leading to a reduction in the sizes of the microparticles. Song *et al.* (2013) evaluated the effect of MF pressure and cycles in the sizes of soy protein particles with sizes between 200 and 120 nm at a MF pressure of 270 MPa by using 1 and 30 MF cycles respectively at pH 7. When working at pH far from the IP, the proteins will have a net charge either positive or negative and the more different the working pH is to the IP, the highest the net charge of the protein (either positive or negative) and, the produced microparticles will be smaller and more stable at pH 3, 7 and 9 than at pH 5. Polydispersity indexes closer to 1 indicated a greater dispersion of particle sizes. On the contrary, values close to zero indicated greater size homogeneity. In the suspensions at pH 3, 5 and 7, there were not significant differences ($p \leq 0.05$) in the PDI values, while in the samples at pH 9 (far from the IP), the PDI decreased significantly with increasing MF cycles from 2 to 3, which indicated greater homogenization efficiency. Additionally, suspensions at pH 9 had smaller particles than those at pH 3, 5 and 7 (Table 1) and the MF reduced and homogenized further the particles at pH 9 since the protein units were strongly negatively charged. Dissayanke *et al*., (2009) reported that MF tends to decrease the particle size distribution.

On the other hand, heating increases the amount of aggregates due to partial denaturation (Shen and Tang, 2012; Dissayanke and Vasiljevic, 2009). In this respect, Song *et al.* (2013) evaluated the particle sizes in microfluidized SPI at similar MF conditions than those used in this work but without heating,

Table 1. Particle size (PS) and polydispersity index (PDI) at different pH values and MF cycles*

pH	MFcycles	PS (μm)	PDI
3	1	0.567±0.009^{a}	0.55±0.09^{a}
	2	0.545±0.017^{ab}	0.51±0.08^{a}
	3	0.539±0.007^{b}	0.51±0.11^{a}
5	1	8.725±0.610^{a}	0.56±0.23^{a}
	2	7.342±0.589^{ab}	0.48±0.04^{a}
	3	6.856±0.470^{b}	0.51±0.18^{a}
7	1	0.531±0.016^{a}	0.37±0.05^{a}
	2	0.467±0.0074^{b}	0.31±0.02^{a}
	3	0.429±0.008^{c}	0.29±0.02^{a}
9	1	0.488±0.011^{a}	0.32±0.02^{a}
	2	0.443±0.009^{b}	0.32±0.04^{a}
	3	0.398±0.004^{c}	0.27±0.01^{b}

*Results are mean values ± SD. Different superscript letters in the same column between pH indicate significant differences ($p \leq 0.05$)

obtaining lower particle sizes than those reported in our work. Dissayanke and Vasiljevic, (2009) when working with whey protein, reported an average PS of 10 μm for pre-heated protein and 1 μm for the non-heated samples. In another work, Shen and Tang, (2012) found that MF greatly improved the solubility and surface hydrophobicity of SPI both, unheated and preheated and reported the formation of new inter-subunit disulfide bonds. The increased PS and surface hydrophobicity can be mostly attributed to the disruption of large insoluble aggregates into smaller soluble ones, due to high shearing during MF (Shen and Tang, 2012).

3.2 Zeta potential

In Table 2, the ζ-P of the suspensions are shown. The lowest values were obtained for the MF microparticles at pH 5. At this pH, just above the IP, only few ionized carboxylic groups were exposed, yielding a negative surface charge in the SPI molecules (Song *et al.,* 2013; Achouri *et al.,* 2005). When increasing number of cycles, no significant differences ($p > 0.05$) were observed in the ζ-P values, at pH 3, 5 and 7 while for pH 9 under 3 cycles, ζ-P showed a significantly higher value. A similar behavior was reported by Gong *et al*. (2019) when increasing the MF pressure above 150 MPa. These results may be due to increased hydrophobicity as cycles increased due the exposure of hydrophobic amino acid residues which are not affected by pH (Lin *et al*., 2012; Peles *et al*., 2012). Our results were similar to those by Liu and Tang (2013) who reported that emulsions stabilized by SPI and formed by MF showed negative

Table 2. ζ-P at different pH values and MF cycles*

pH	MF cycles	ζ-P (mV)
3	1	-34.50±1.20^{a}
	2	-35.12±1.50^{a}
	3	-34.80±1.10^{a}
5	1	-22.58±0.06^{c}
	2	-23.70±1.00^{c}
	3	-23.78±0.89^{c}
7	1	-32.11±1.40^{a}
	2	-31.05±1.70^{a}
	3	-32.20±1.60^{a}
9	1	-32.40±1.80^{a}
	2	-31.50±1.70^{a}
	3	-29.40±2.40^{b}

*Results are mean values ± SD. Different superscript letters in the same column indicate significant differences ($p \leq 0.05$).

ζ-Ps (from -8 to -25 mV). At pH values close to the IP, ζ-P values will be closer to zero than at pH far from the IP due to increased charge-balance of the microparticles. Therefore, the samples at pH 5 were the most unstable depicting the largest values of ζ-P (Table 2). The greater the dispersing force, the more stable the suspensions become and, in general, values of $|\zeta\text{-P}| \geq 30$ mV are indicative of electric charge-stability of the system (Villalobos-Espinosa *et al.,* 2019; Quintanilla-Carvajal *et al.,* 2011).

A consequence of high-pressure treatments is the exposure of electrically charged groups on the surface of the protein (Chen *et al.,* 2016). Results obtained by Song *et al.* (2013) showed an increase in the negative ζ-P values in soy protein aggregates (from -16mV to -26mV) by increasing the number of MF cycles (from 1 to

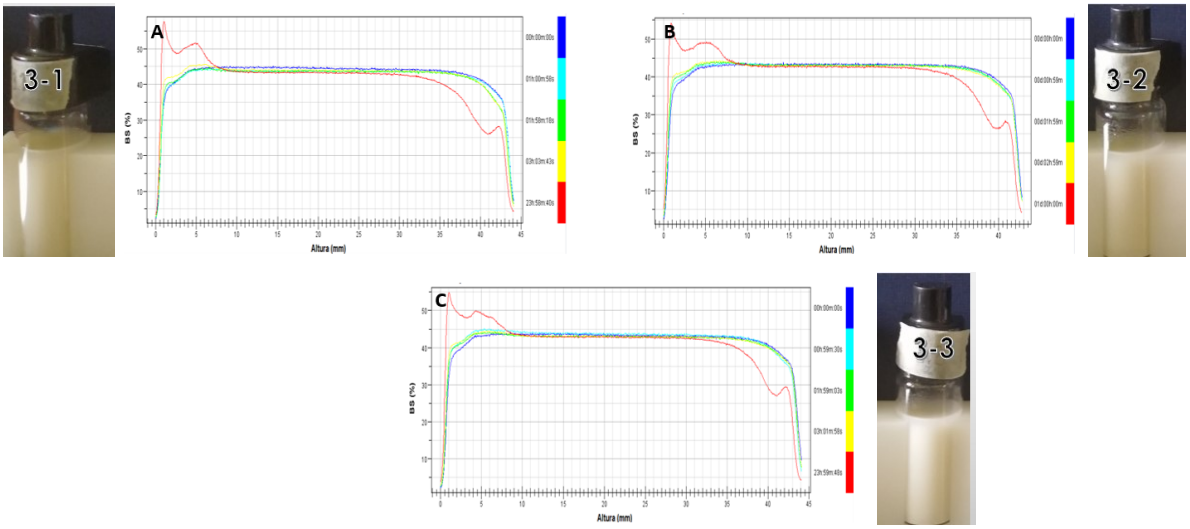

Fig. 1. Backscattering profile (BS) as a function of time (24h) and height of the sample volume (45mm) in the suspension of microparticles at pH 3 A) 1 MF cycle B) 2 MF cycles C) 3 MF cycles. Macroscopic images of soy protein microparticles suspensions at pH 3 after 24h. (3-1):1 MF cycle; (3-2): 2 MF cycles; (3-3): 3 MF cycles.

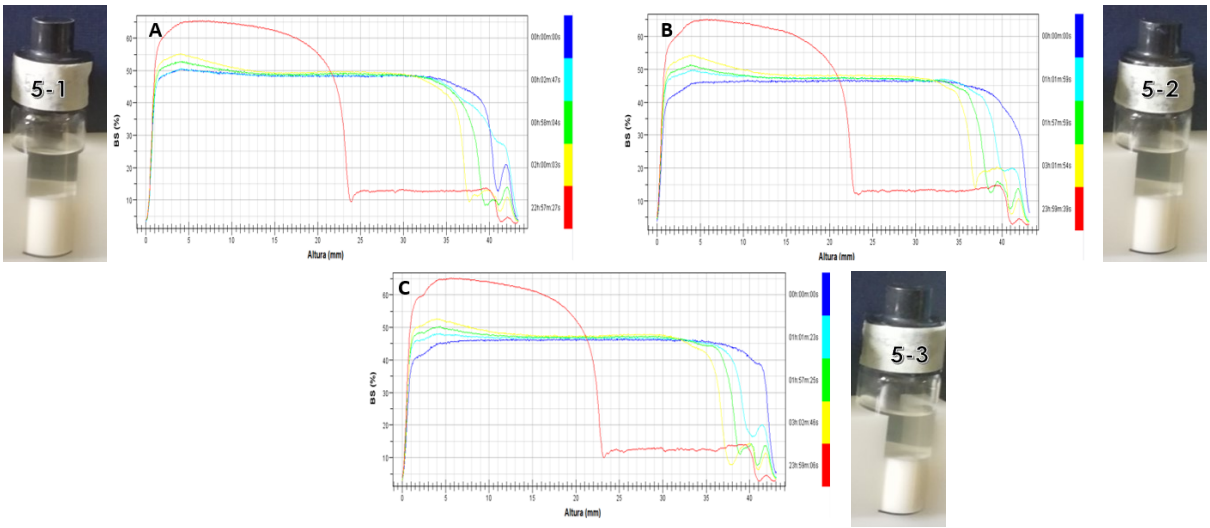

Fig. 2. Backscattering profile (BS) as a function of time (24h) and height of the sample volume (45mm) in the suspension of microparticles at pH 5 A) 1 MF cycle B) 2 MF cycles C) 3 MF cycles. Macroscopic images of soy protein microparticles suspensions at pH 5 after 24h. (3-1):1 MF cycle; (3-2): 2 MF cycles; (3-3): 3 MF cycles.

30) which indicated that MF had a positive effect on the reduction of particle size as well as on promoting inter-particle repulsions due to the exposition of charged amino acid, which caused greater electrical stability of the system. In the case of peanut protein, Gong *et al.* (2019) found that, when increasing the pressure from 0.1 to 120 MPa, the ζ-P varied from -34 to -39mV, and at pressures greater than 150 MPa, the ζ- P was -34mV, which indicated disaggregation of the protein when processed at pressures lower than 120 MPa and reaggregation at pressures greater than 150MPa.

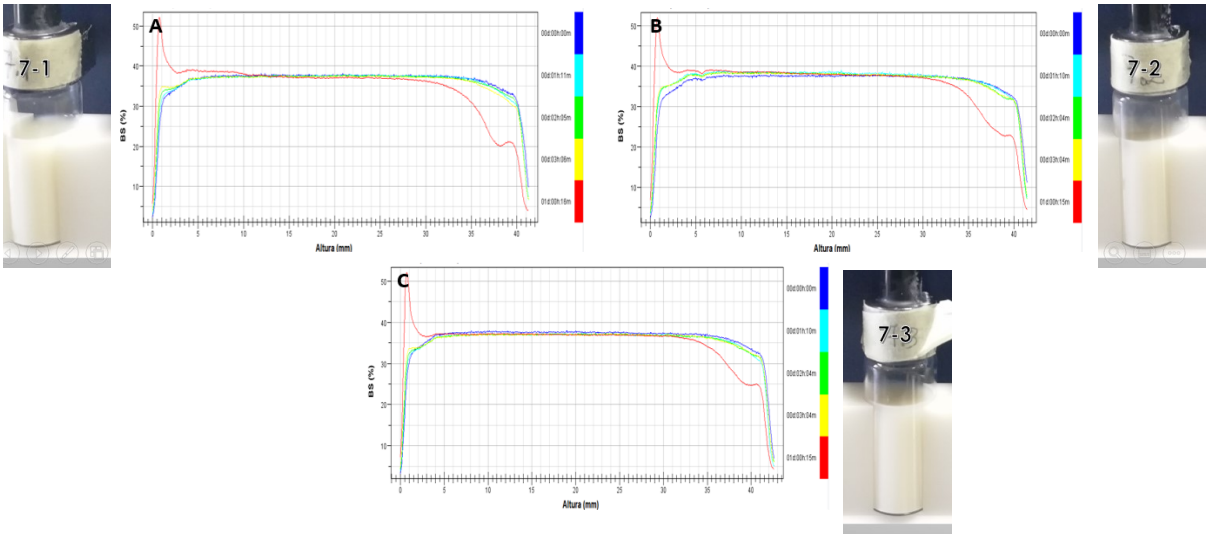

Fig. 3. Backscattering profile (BS) as a function of time and height of the sample for suspension of microparticles at pH 7. A) 1 MF cycle B) 2 MF cycles C) 3 MF cycles. Macroscopic images of soy protein microparticles suspensions at pH 7 after 24h. (3-1):1 MF cycle; (3-2): 2 MF cycles; (3-3): 3 MF cycles.

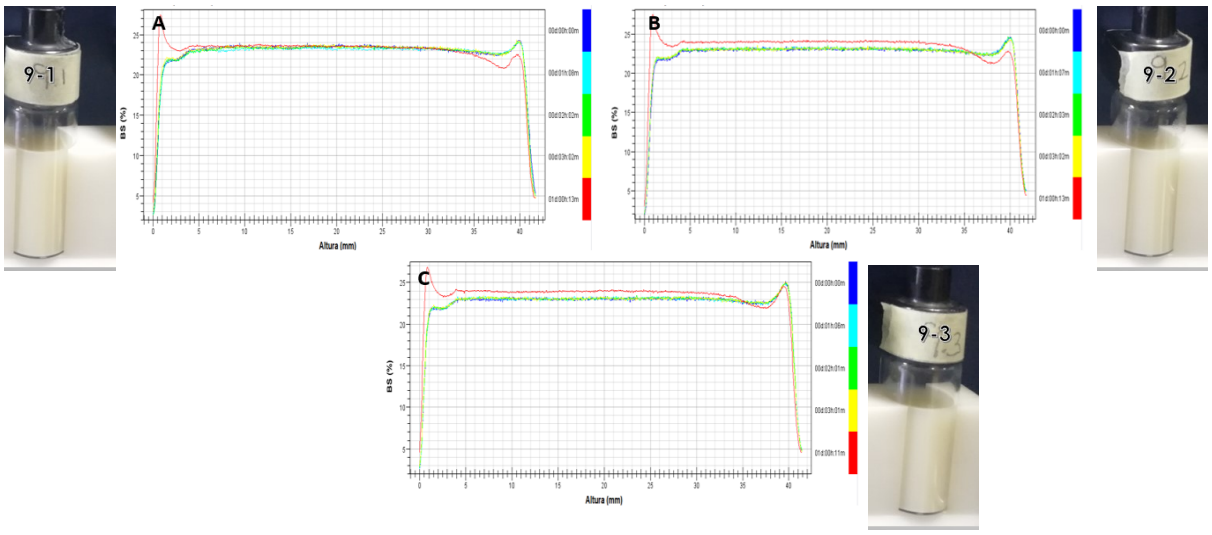

Fig. 4. Backscattering profile (BS) as a function of time and height of the sample for suspension of microparticles at pH 9. A) 1 MF cycle B) 2 MF cycles C) 3 MF cycles. Macroscopic images of soy protein microparticles suspensions at pH 9 after 24h. (3-1):1 MF cycle; (3-2): 2 MF cycles; (3-3): 3 MF cycles.

3.3 Turbiscan Stability Index (TSI)

The backscattering profiles and images of the appearance of MF suspensions after 24 h of preparation are shown in Figures 1 to 4 for the different pH treatments. For samples at pH 3, it was observed that during the first 3 h, non-significant changes in the profiles were observed, but that after 24 h, phase separation was noted. The same trend was observed at pH 7 and 9 (Figures 3 and 4). In suspensions at pH 9, the profile after 24 h showed a much milder departure from the profile at 3 h than the other samples. The backscattering data were corroborated by the visual inspection of the macroscopic appearances of the suspensions left to stand during 24 h in Turbiscan tubes (Figures 1-4). Thus, the SPI suspension at pH 9 and treated at 1 MF cycle can be considered the most

Table 3. Turbiscan stability index (TSI) for suspension of microparticle at different pH values and MF cycles at 24h*

pH	MF cycles	TSI
3	1	3.9 ± 0.0^{a}
	2	3.4 ± 0.0^{b}
	3	3.2 ± 0.0^{c}
5	1	47.7 ± 1.1^{b}
	2	53.0 ± 1.2^{a}
	3	54.0 ± 1.8^{a}
7	1	3.3 ± 0.0^{a}
	2	2.9 ± 0.0^{b}
	3	2.3 ± 0.0^{c}
9	1	0.8 ± 0.1^{b}
	2	1.1 ± 0.0^{a}
	3	1.1 ± 0.0^{a}

*Results are mean values ± SD. Different superscript letters in the same column between pH indicate significant differences ($p \leq 0.05$)

stable, as it showed the lowest backscattering and macroscopic separation after 24 h (Figure 4; Image 3-3). As expected, the most unstable MF dispersion was at pH 5, which exhibited the largest backscattering profile change between 3 and 24 h of aging (Figure 2; images 3-1, 3-2, 3-3) and the largest macroscopic visual separation after 24 h. These results were in close agreement with the PS and PDI data shown in Table 1. The smaller the PS and the PDI, the greater the stability against phase separation of the suspensions. The data of the backscattering profiles were analyzed to obtain a quantitative measure of suspesion stability of the suspensions versus phase separation, i.e., the TSI. The TSI values for the 24 h aged suspensions are given in Table 3 as a function of pH and MF cycles. Depending on the differences in charge between media and microparticles, they will tend to sediment over time. When particles were suspended in media which pH is far (3, 7 and 9) to the IP of the SPI, particles repeled each other improving their stability in suspension (González-Cruz *et al*., 2020). However, at pH value close (5) to the IP, particles tended to sediment since reduced repulsion forces will exist between media and their surface. The structural changes will be also promoted by MF which induced unfolding of the protein chains (Liu and Kuo, 2016; Hu *et al*., 2011). At pH 9, the TSI value was lower for 1 cycle than for 2 and 3 cycles, and this result is seemingly in contradiction with the trend in particle size that was smaller the more cycles were applied. This could be a signal of overprocessing by MF when by increasing the number of cycles or pressure, the PS and TSI increasd due to the reaggregation of the protein. This effect was observed in zein when increasing the pressure of MF (from 75 to 100 MPa for 3 cycles) the PS increased from 60nm to 100 nm (Sun *et al.,* 2016). At pH 9, the largest amount of deprotonated carboxylic groups was exposed to the media and helped maintaining the particles in suspension thus decreasing the TSI values. Additionally, ζ-P values were larger for suspensions at pH 5 which was due to the proximity to the IP of the SPI.

One of the traditional techniques for obtaining microparticles is by increasing temperature and modifying the pH (Ipsen, 2016) and, as previously commented, the highest concentration of aggregates occurs at temperatures above 90 °C during at least 15 min (Chen *et al.,* 2017). The samples at pH 5 had the largest size, ζ-P and TSI indicating reduced stability compared to suspensions at pH values far from the average IP of SPI (4.5). At pH 3 and 9 (far from IP), the SPI globular structure unfolded and exposed ammonia and carboxylic groups respectively.

However, the TSI embraces all phenomena taking place in the sample leading to destabilization (Qi *et al*., 2017), i.e., continuous phase viscosity, ζ-P, etc. Low TSIs (close to zero) indicated greater suspension stability (Kang *et al.,* 2011). Li *et al.,* (2020) analyzed the stability in soy milk produced by MF. Their results indicated that samples remained practically stable (without sedimentation and/or creaming) during 21 days in refrigerated conditions (4°C). They also found that the particle size practically did not increase during the cold storage.

In addition to the effect of pH, the high pressures applied during MF provokes denaturation of the proteins causing the formation of a new network with larger particle sizes of the aggregates (Liu and Kuo, 2016) causing flocculation of the microparticles. This effect may be related to the intense exposure of hydrophobic sites caused by the application of high pressures and shear forces in the interaction chambers which can modify the structure of the proteins. These phenomena have been reported in soy proteins (Liu and Kuo, 2016), trypsin (Liu *et al.,* 2010), and peanut protein (Hu *et al.,* 2011).

Table 4. Surface roughness results by AFM in SPI during microparticulation process*

Sample	Ra (nm)	Rq (nm)	Sample	Ra (nm)	Rq (nm)
pH3	5.60 ± 1.38^{b}	6.89 ± 1.4^{b}	pH5	2.77 ± 0.46^{c}	4.42 ± 1.06^{c}
pH3-H	5.67 ± 1.17^{b}	7.09 ± 1.79^{b}	pH5-H	3.18 ± 0.09^{c}	4.08 ± 0.24^{c}
pH3-1MFC	8.19 ± 2.13^{a}	9.27 ± 3.2^{b}	pH5-1MFC	17.3 ± 1.41^{a}	21.0 ± 0.99^{a}
pH3-2MFC	8.47 ± 2.42^{a}	14.05 ± 3.8^{a}	pH5-2MFC	6.9 ± 1.61^{b}	8.56 ± 2.74^{b}
pH3-3MFC	4.28 ± 0.74^{b}	5.80 ± 0.80^{b}	pH5-3MFC	6.78 ± 1.41^{b}	8.46 ± 0.99^{b}
pH7	5.71 ± 0.89^{a}	6.70 ± 0.87^{b}	pH9	10.95 ± 1.20^{a}	13.85 ± 0.64^{a}
pH7-H	4.85 ± 0.59^{b}	9.63 ± 3.83^{a}	pH9-H	6.60 ± 1.42^{b}	8.61 ± 1.06^{b}
pH7-1MFC	3.39 ± 0.48^{c}	6.22 ± 1.94^{b}	pH9-1MFC	5.25 ± 0.95^{c}	6.69 ± 0.74^{c}
pH7-2MFC	3.46 ± 0.44^{c}	4.90 ± 0.58^{c}	pH9-2MFC	6.30 ± 0.92^{b}	8.51 ± 0.18^{b}
pH7-3MFC	5.86 ± 1.11^{a}	11.73 ± 1.04^{a}	pH9-3MFC	5.18 ± 0.16^{c}	8.34 ± 1.61^{b}

*Results are mean values ± SD. Different superscript letters in the same column between pH indicate significant differences ($p \leq 0.05$). Ra (arithmetic mean roughness) Rq (mean square roughness). pH: SPI agreggates by the effect of pH; pH-H: SPI aggregates after heat treatment; pH-1MFC: SPI microparticles after 1 MF cycle; pH-2MFC: SPI microparticles after 2 MF cycles; pH-2MFC: SPI microparticles after 3 MF cycles.

It has been reported that, during MF, enough energy is supplied to the feed to break the polymer structure into subunits by altering hydrogen bonding, hydrophobic, hydrophilic and electrostatic interactions, modifying the structure in the protein network (Song *et al*., 2013; Tang *et al*., 2009). The higher the pressure and duration of treatment, the larger the extent at which bonds will break and globular structures unfold exposing functional groups interacting with the media. On the other hand, it would be expected that MF caused changes in the polar environment and an increment of surface hidrophobicity and in disulfide bonds (Gong *et al*., 2019).

3.4 Surface roughness

Surface roughness of AFM images indicates the extent of dispersion of the microparticles in the examined samples. In Table 4, the results of the surface roughness analysis are shown. In samples at pH 3, the Ra (arithmetic mean roughness) and Rq (mean square roughness) increased when the samples were subjected to two MF cycles and the larger values of roughness were obtained at pH 5 and 1 MF cycle. In samples at pH 7 and 9, the values of the roughness decreased significantly ($p \leq 0.05$) after MF. The observed decrement was, probably related to the increased affinity of microparticles with suspension media given the exposure of deprotonated carboxylic groups causing a greater number of homogeneously dispersed microparticles in the AFM image which caused decreased roughness. Acosta-Dominguez *et al*. (2016) when studying the changes in surface roughness in nanostructured SPI, found that the reduction of particle size could decrease the roughness of SPI due to nanostructuration by immersing samples in cryogenic fluids at -50°C.

In Figures 5 (samples at pH 3 and 5) and 6 (samples at pH 7 and 9), the 2D AFM images obtained in the peak force error channel (channel in which images with the best delimited shapes were observed) are presented. In images (B, G, B1, G1) the effect of exposure to high temperature was noted by displaying larger amounts of big aggregates which decreased their sizes after the MF. In images A1-J1 (Figure 6), it was possible to observe the presence of a higher amount of smaller and more evenly distributed microparticles than in images A-J (Figure 5) at pH 7 and 9 which could be due to a higher exposure of charged amino acid residues. AFM images were useful to observe the similitudes of the microparticles formed after the MF process at pH 3, 7 and 9 (far from the IP) being the main differences between them other variables such as PS and PDI, described in Sections 3.1, TSI (Section 3.3) and Texture image analysis (Section 3.5). In terms of surface roughness, the main differences amongst them were the heights of the profiles as described below (Figure 7). Zhong *et al*., (2012) evaluated by AFM the morphological changes in β-LG subjected to different MF pressures (0.1-180 MPa), finding a decrease in particle size of the aggregates when increasing MF pressures. Oboroceanu *et al*., (2010) observed the aggregation of β-lactoglobulin due to heating at different times by using AFM images.

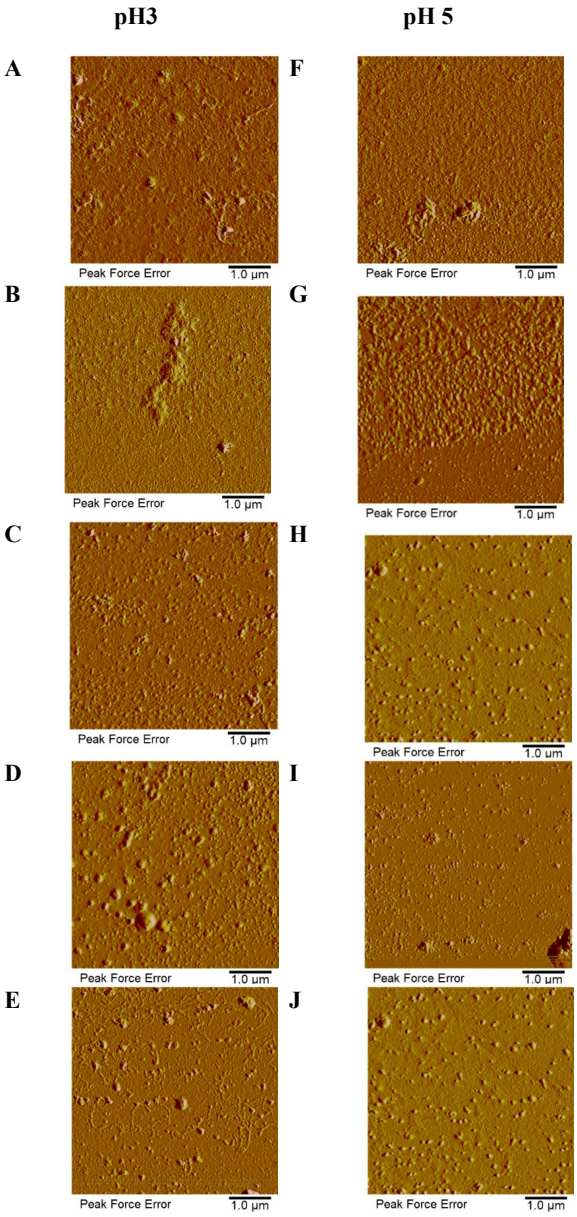

Fig. 5. AFM SPI micrographs during the microparticulation process A) SPI aggregates at pH 3 B) SPI aggregates at pH3 after heat treatment C) SPI microparticles after 1 cycle of MF at pH 3 D) SPI microparticles after 2 cycles of MF at pH3 E) SPI microparticles after 3 cycles of MF at pH3 F) SPI aggregates at pH 5 G) SPI aggregates at pH5 after heat treatment H)) SPI microparticles after 1 cycle of MF at pH 5 I) SPI microparticles after 2 cycles of MF at pH 5 J) SPI microparticles after 3 cycles of MF at pH 5.

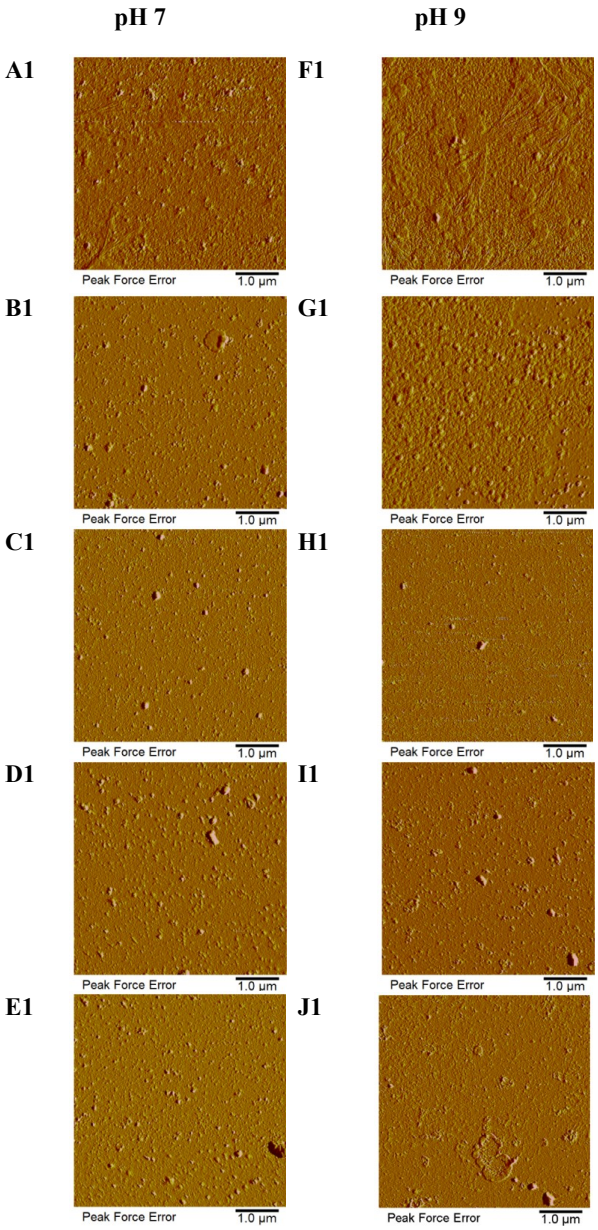

Fig. 6. AFM SPI micrographs during the microparticulation process A1) SPI aggregates at pH 7 B1) SPI aggregates at pH 7 after heat treatment C1) SPI microparticles after 1 cycle of MF at pH 7 D1) SPI microparticles after 2 cycles of MF at pH 7 E1) SPI microparticles after 3 cycles of MF at pH7 F1) SPI agreggates at pH9 G1) SPI aggregates at pH9 after heat treatment H1) SPI microparticles after 1 cycle of MF at pH 9 I1) SPI microparticles after 2 cycles of MF at pH 9 J1) SPI microparticles after 3 cycles of MF at pH 9.

Figure 7 shows the AFM height profiles of the surface of the SPI before and after MF. In all cases, a decrease in height was observed after MF, which confirmed the reduction in particle size of the microparticles compared to the initial aggregates. The maximum heights registered in the surface images by AFM were 1.1, 1.2, 1.1, and 0.28 μm for the samples at pH values 3, 5, 7, and 9 respectively as shown in Figures A8, C8, E8 and G8. These heights decreased after 3 MF cycles to 0.990, 0.628, 0.541, and 0.082 μm as shown in Figures B8, D8, F8 and H8. In the case of microparticles at pH 3 and 7,

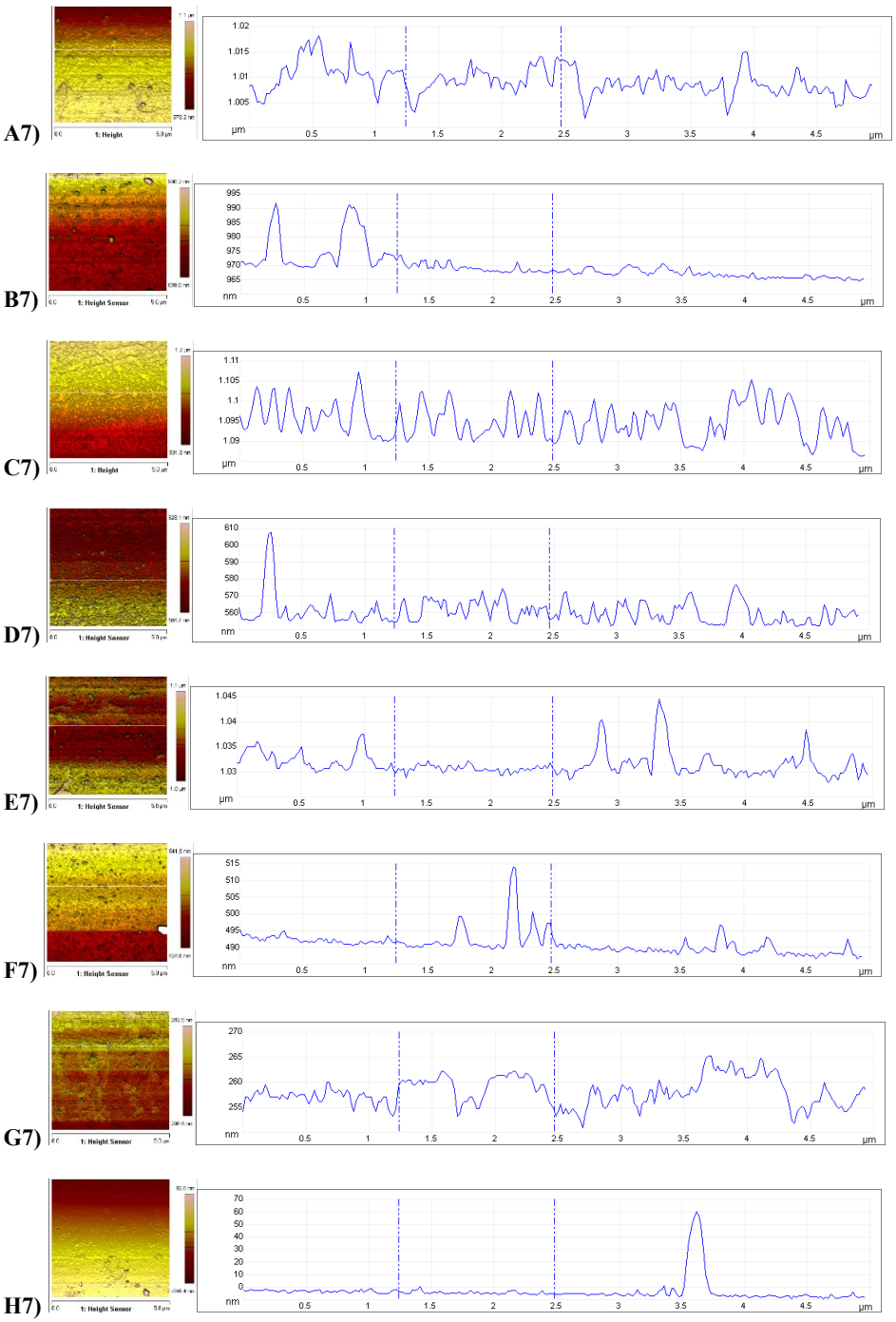

Fig. 7. AFM height profiles of the surface of SPI (section size is 5 μm). A7) SPI aggregates before MF at pH3. B7) SPI microparticles at pH3 after 3 cycles of MF. C7) SPI aggregates before MF at pH5. D7) SPI microparticles at pH5 after 3 cycles of MF. E7) SPI aggregates before MF at pH7. F7) SPI microparticles at pH7 after 3 cycles of MF. G7) SPI aggregates before MF at pH9. H7) SPI microparticles at pH9 after 3 cycles of MF.

evaluated heights were similar to the particle sizes determined by dynamic light scattering (Section 3.1) and slightly lower for the microparticles at pH 5 and 9. These findings indicated that AFM profiles may be considered as a valuable tool to describe the sizes of microparticles in conjunction with DLS tests (Section 3.1) and complemented with textural image analysis (Section 3.5). Li *et al*., (2020) characterized the fibril formation in cowpea, chickpea, and lentil proteins by using AFM, and evaluated the changes in the fibril's dimensions at different heat treatment times as a function of the height and contour length of the images. The characterization of the surface of proteins aggregates could be related to their capacity to interact with other compounds such as water or oil (Bildyukevich *et al*., 2020; Wen *et al*., 2020). In this work, the smallest microparticles were obtained at pH 9 (Figure H7) and 3 MF cycles and were more stable due to water-protein interactions. Acosta-Dominguez *et al*. (2016) found that interactions between the nanostructured soy protein and water, increased with the number of nanocavities on the surface of particles, which was reflected in higher water holding capacities and better gelling properties. These authors also reported that interactions between proteins and water decreased at pH values close to the IP of the protein.

3.5 Texture image analysis

Table 5 shows the results of texture parameters angular second moment, contrast, correlation, inverse difference moment, entropy, and fractal dimension. Only the second angular moment correlated well with the image texture of the microparticles in the whole range of MF conditions and pretreatments. This parameter indicates the texture uniformity or orderliness of an image (Hernández-Carrión *et al*., 2015; Barrera *et al.,* 2013; Ou *et al.,* 2014) and in this respect, an increment in its value was observed when increasing the number of MF cycles, indicating greater homogeneity of the texture of the analyzed images and may be considered an appropriate descriptor of their texture (Yang *et al*., 2000). In a study carried out by Yang *et al*. (2000), it was concluded that the angular second moment was a good descriptor of the structure of biofilms. The other texture parameters (contrast, inverse difference moment, correlation, entropy, and fractal dimension) did not correlate with the characteristics of the images within the whole range of operating conditions given that their texture calculation algorithms were not sensitive enough to detect the small variations in texture (Qiao, *et al*., 2007; Laddi *et al.,* 2013). In this respect, the contrast of the images of particles obtained by applying 3 MF cycles at pH 7 decreased significantly ($p \leq 0.05$). Contrast, measures of the intensity of the differences between a pixel and its neighbor over the whole image and is considered a dynamic range of gray level or sharpness of edges (Laddi *et al.,* 2013). The inverse difference moment (IDM) increased in samples after 3 cycles of MF which corresponded to the microparticles with lower PDI, except for samples at pH 7. Hernández-Carrión *et al.,* (2015), analyzed the changes in the texture parameters in images obtained by SEM in red sweet pepper subjected to high pressure processing and observed that IDM depended on the magnification of the images to be analyzed. Correlation of the obtained images did not show any relationship to MF conditions and these results were consistent with findings by Hernández-Carrión *et al.,* (2015) who did not obtain significant changes in this parameter in relation to images of the structural changes in red sweet pepper tissue after high pressure processing. The entropy of the images did not change significantly ($p > 0.05$) in the different stages of microparticulation. The entropy is a statistical measure of randomness of the object that can be used to characterize the texture of the input image. This finding indicated that the microparticles having relatively similar values of rugosity (Section 3.4) were dispersed in the image by following similar patterns amongst samples due to charge-related characteristics such as those reported in Section 3.1.

The fractal dimension of texture (FDt) did not show any significant ($p > 0.05$) changes with operating conditions for samples at pH 5 and 9. On the other hand, in the pH 3 samples, the FDt values decreased after the MF process. Several studies have concluded that higher values of FDt indicate rougher and more irregular surfaces with notorious differences in the gray-scale levels of the image and could indicate disorganized distribution of particles in the samples (Arzate-Vázquez *et al*., 2012; Alvarado-González *et al*. , 2012). In relation to all treatments, the FDt values remained practically constant given that the fractal dimension is a logarithmic variable and changes little with small texture variations (Quintanilla-Carvajal *et al*., 2011). These results indicated that the irregularities of the images were similar and analogous amongst them mainly due to homogeneous distributions of microparticles in the suspensions and that the differences in sizes and PDI given in Section 3.1 and Surface rugosity (Section 3.4) could not be detected by the fractal dimension algorithm.

Table 5. Texture image analysis during the SPI microparticulation process.

Sample	Angular second moment	Contrast	Correlation	Inverse difference moment	Entropy	Fractal Dimension (FDt)
pH3	0.0004 ± 0.0^{e}	347.9 ± 12.2^{b}	0.001 ± 0.0^{b}	0.10 ± 0.0^{a}	8.3 ± 0.2^{a}	1.9 ± 0.0^{a}
pH3-H	0.0169 ± 0.0^{a}	518.5 ± 19.5^{a}	0.001 ± 0.0^{b}	0.14 ± 0.1^{a}	8.1 ± 0.8^{a}	1.9 ± 0.0^{a}
pH3-1MF	0.0009 ± 0.0^{d}	251.7 ± 12.5^{c}	0.001 ± 0.0^{b}	0.12 ± 0.0^{a}	7.9 ± 0.4^{a}	1.9 ± 0.0^{a}
pH3-2MF	0.0017 ± 0.0^{b}	175.5 ± 16.2^{e}	0.002 ± 0.0^{a}	0.19 ± 0.1^{a}	7.6 ± 0.5^{a}	1.6 ± 0.2^{b}
pH3-3MF	0.0012 ± 0.0^{c}	215.6 ± 13.4^{d}	0.001 ± 0.0^{b}	0.14 ± 0.1^{a}	7.6 ± 0.7^{a}	1.6 ± 0.4^{b}
pH5	0.0008 ± 0.0^{b}	454.3 ± 31.4^{a}	0.001 ± 0.0^{b}	0.11 ± 0.1^{a}	8.1 ± 0.4^{a}	1.9 ± 0.1^{a}
pH5-H	0.0007 ± 0.0^{c}	405.0 ± 16.7^{b}	0.001 ± 0.0^{b}	0.11 ± 0.0^{d}	8.1 ± 0.2^{a}	1.9 ± 00^{a}
pH5-1MF	0.0014 ± 0.0^{a}	253.9 ± 11.2^{d}	0.001 ± 0.0^{b}	0.15 ± 0.0^{b}	7.5 ± 0.4^{b}	1.8 ± 0.2^{a}
pH5-2MF	0.0014 ± 0.0^{a}	346.2 ± 39.8^{c}	0.001 ± 0.0^{b}	0.13 ± 0.0^{c}	7.7 ± 0.5^{a}	1.8 ± 0.2^{a}
pH5-3MF	0.0014 ± 0.0^{a}	243.9 ± 17.6^{d}	0.002 ± 0.0^{a}	0.16 ± 0.0^{a}	7.5 ± 0.4^{b}	1.7 ± 0.2^{a}
pH7	0.0004 ± 0.0^{c}	361.5 ± 71.1^{c}	0.001 ± 0.0^{b}	0.10 ± 0.0^{d}	8.3 ± 0.1^{a}	1.9 ± 0.0^{c}
pH7-H	0.0008 ± 0.0^{a}	208.3 ± 29.0^{d}	0.002 ± 0.0^{a}	0.14 ± 0.0^{a}	7.9 ± 0.2^{a}	1.9 ± 0.0^{b}
pH7-1MF	0.0006 ± 0.0^{b}	574.7 ± 23.5^{a}	0.001 ± 0.0^{b}	0.09 ± 0.0^{d}	8.1 ± 0.1^{a}	1.9 ± 0.0^{a}
pH7-2MF	0.0008 ± 0.0^{a}	473.9 ± 31.6^{b}	0.001 ± 0.0^{b}	0.11 ± 0.0^{b}	8.0 ± 0.4^{a}	1.9 ± 0.0^{a}
pH7-3MF	0.0008 ± 0.0^{a}	429.7 ± 15.9^{c}	0.001 ± 0.0^{b}	0.11 ± 0.0^{b}	7.8 ± 0.3^{a}	1.8 ± 0.1^{a}
pH9	0.0003 ± 0.0^{d}	748.6 ± 36.1^{a}	0.001 ± 0.0^{b}	0.07 ± 0.0^{e}	8.5 ± 0.1^{a}	1.9 ± 0.0^{a}
pH9-H	0.001 ± 0.0^{b}	593.5 ± 37.7^{b}	0.001 ± 0.0^{b}	0.10 ± 0.0^{c}	8.1 ± 0.6^{a}	1.8 ± 0.2^{a}
pH9-1MF	0.001 ± 0.0^{b}	601.3 ± 24.4^{b}	0.001 ± 0.0^{b}	0.09 ± 0.0^{d}	7.9 ± 0.2^{a}	1.9 ± 0.0^{a}
pH9-2MF	0.001 ± 0.0^{b}	297.1 ± 26.5^{c}	0.001 ± 0.0^{b}	0.14 ± 0.0^{a}	7.6 ± 0.2^{a}	1.9 ± 0.0^{a}
pH9-3MF	0.002 ± 0.0^{a}	280.6 ± 16.8^{c}	0.001 ± 0.0^{b}	0.14 ± 0.0^{a}	7.5 ± 0.6^{a}	1.7 ± 0.2^{a}

*Results are mean values ± SD. Different superscript letters in the same column between pH indicate significant differences ($p \leq 0.05$). pH: SPI aggregates by the effect of pH; pH-H: SPI aggregates after heat treatment; pH-1MFC: SPI microparticles after 1 MF cycle; pH-2MFC: SPI microparticles after 2 MF cycles; pH-2MFC: SPI microparticles after 3 MF cycles.

Conclusions

Suspensions at pH 9 presented the smallest particle size ($0.398 \pm 0.004\ \mu$m) after being subjected to 3 MF cycles, and the lowest TSI (0.8 ± 0.1) when subjected to 1 MF cycle. Therefore, most stable suspension against phase separation as given by the TSI were obtained at pH 9 and 1 MF cycle. In general, the stability of the SPI suspensions decreased, as the pH of the suspension was nearer that of the average IP (4.5) of the proteins. By atomic force microscopy it was possible to observe the breakdown of the aggregates for the formation of microparticles and height of the obtained peaks of the roughness profiles (heights) were rather well descriptors of the size of the microparticles. Surface roughness and image texture analyses allowed the evaluation of the effect of MF on the surface of the microparticles. In samples at pH 7 and 9, the values of the roughness decreased significantly ($p \leq 0.05$) after MF. The observed decrement was, probably related increased affinity of microparticles with suspension media due to the exposure of deprotonated carboxylic groups causing homogeneously dispersed microparticles in the AFM image which gave place to decreased roughness. The most relevant descriptor for their characterization was the second angular moment whereas contrast, inverse difference moment, correlation, entropy, and fractal dimension did not correlate with the characteristics of the images in the whole range of operating conditions given that their calculation algorithms are not sensitive enough as to detect the variations in the roughness of the samples. The best conditions for microparticles production were 1 MF cycle and pH 9 in accordance with the Turbiscan stability index that encompasses the contributions of different factors to instability.

Acknowledgements

Author I. Monroy-Rodríguez, thanks CONACYT (Mexico) and IPN (Mexico) for support in the form of PhD study grants. Authors thank CONACYT and IPN for funding this research under CONACYT (CB-242371) and IPN (20171502, 20181587, 20196167, 20201678) grants.

Nomenclature

SPI	Soy protein isolate
MF	Microfluidization
TSI	Turbiscan stability index
AFM	Atomic force microscopy
IXC	Interaction chamber
PS	Particle size
PDI	Polidispersity Index
IP	Isoelectric point

References

Achouri, A., Boye, J.I., Yaylayan, V.A. and Yeboah, F.K. (2005). Functional properties of glycated soy 11s glycinin. *Journal of Food Chemistry and Toxicology* 70(4), 269-274. https://doi.org/10.1111/j.1365-2621.2005.tb07172.x

Acosta-Domínguez, L., Hernández-Sánchez, H., Gutiérrez-López, G. F., Alamilla-Beltrán, L. and Azuara, E. (2016). Modification of the soy protein isolate surface at nanometric scale and its effect on physicochemical properties. *Journal of Food Engineering* 168, 105-112. https://doi.org/10.1016/j.jfoodeng.2015.07.031

Alvarado-González, J.S., Chanona-Pérez, J.J., Welti-Chanes, J. S., Calderón-Domínguez, G., Arzate-Vázquez, I., Pacheco-Alcalá, S. U., Garibay-Febles, V. and Gutiérrez-López, G. F. (2012). Optical, microstructural, functional and nanomechanical properties of aloe vera gel / gellan gum edible films. *Revista Mexicana de Ingeniería Química*, 11(2), 193-210. http://rmiq.org/iqfvp/Pdfs/Vol.%2011,%20No.%202/Alim1/Alim1.pdf

AOAC (Association of Official Agricultural Chemists) (1984). Official Methods of Analysis. Kjeldahl method (2.062). 14th edition. Washington D.C., USA.

Arzate-Vázquez, I., Chanona-Pérez, J. J., Calderón-Domínguez, G., Terres-Rojas, E., Garibay-Febles, V., Martínez-Rivas, A. and Gutiérrez-López, G.F. (2012). Microstructural characterization of chitosan and alginate films by microscopy techniques and texture image analysis. *Carbohydrate Polymers* 87(1), 289-299. https://doi.org/10.1016/j.carbpol.2011.07.044

Barrera, G.N., Calderón-Domínguez, G., Chanona-Pérez, J., Gutiérrez-López, G.F., Leóna, A.E. and Ribottab, P.D., (2013). Evaluation of the mechanical damage on wheat starch granules by SEM, ESEM, AFM and texture image analysis. *Carbohydrate Polymers* 98 (2), 1449-1457. https://doi.org/10.1016/j.carbpol.2013.07.056

Bernewitz, R., Guthausen, G., and Schuchmann, H.P. (2011). NMR on emulsions: characterization of liquid dispersed systems. *Magnetic Resonance in Chemistry* 49, 93-104. https://doi.org/10.1002/mrc.282

Bildyukevich, A. V., Plisko, T. V., Lipnizki, F., and Pratsenko, S. A. (2020). Correlation between membrane surface properties, polymer nature and fouling in skim milk ultrafiltration. *Colloids and Surfaces A: Physicochemical and Engineering Aspects 605*, 125387. https://doi.org/10.1016/j.colsurfa.2020.125387

Cano-Sarmiento, C., Alamilla-Beltrán, L., Azuara-Nieto, E., Hernández-Sánchez, H., Téllez-Medina, D. I., Jiménez- Martínez, C. and Gutiérrez-López, G. F. (2015). High shear methods to produce nano-sized food related to dispersed systems. In: Food Nanoscience and Nanotechnology (Hernández-Sánchez H., Gutiérrez-López G. eds). Pp 145-161. Food Engineering Series. Springer, Cham. https://doi.org/10.1007/978-3-319-13596-0_8

Chen, W., Yuan, S., Hsiao, H. and Hsieh, C. (2001). Algorithms to estimating fractal dimension of texture images. IEEE International Conference on Acoustics, Speech and Signal Processing, Vol. 3. Pp. 1541-1544. Hong Kong, China.

Chen, X., Xu, X. and Zhou, G. (2016). Potential of high-pressure homogenization to solubilize chicken breast myofibrillar proteins in water. *Innovative Food Science Emerging Technology 33*, 170-179. https://doi.org/10.1016/j.ifset.2015.11.012

Chung, C., Degner, B. and McClements, D.J. (2014). Development of reduced-calorie foods:

microparticulated whey proteins as fat mimetics in semi-solid food emulsions. *Food Research International* 56, 136-45. https://doi.org/10.1016/j.foodres.2013.11.034

Dissanayake, M., Alan L. K. and Vasiljevic, T. (2010). Gelling properties of microparticulated whey proteins. *Journal of Agricultural and Food Chemistry* 58(11), 6825-32. https://doi.org/10.1021/jf1009796

Dissanayake M., and Vasiljevic T. (2009). Functional properties of whey proteins affected by heat treatment and hydrodynamic high-pressure shearing. *Journal of Dairy Science*, 92(4), 1387-1397. https://doi.org/10.3168/jds.2008-1791

Formulation Smart Scientific Analysis (2021). Static multiple light scattering (SMLS). Available at: https://www.formulaction.com/en/productsandtechnologies/technologies/static-multiple-light-scattering-s-mls. Accessed: January 25, 2021.

Gong, Kuijie, Lirong Chen, Haiyong Xia, Hongcui Dai, Xiaoyue Li, Linlin Sun, Weilin Kong, and Kaichang Liu. (2019). Driving forces of disaggregation and reaggregation of peanut protein isolates in aqueous dispersion induced by high-pressure microfluidization. *International Journal of Biological Macromolecules* 130, 915-21. https://doi.org/10.1016/j.ijbiomac.2019.02.123

Gong, K., Deng, L., Shi, A., Liu, H., Liu, L., Hui, H., Adhikari, B. and Wang, Q. (2017). High-pressure microfluidisation pretreatment disaggregate peanut protein isolates to prepare antihypertensive peptide fractions. *International Journal of Food Science and Technology* , *52*(8), 1760-1769. https://doi.org/10.1111/ijfs.13449

González-Cruz, L., Juárez-Goiz, J., Teniente-Martínez, G., Acosta-García, G., Flores-Martínez, N., and Bernardino-Nicanor, A. (2020). Structural changes in the proteins from two species of the genus vigna by effect of different treatments.*Revista Mexicana de Ingeniería Química*,*19*(Sup. 1), 333-347. https://doi.org/10.24275/rmiq/Alim1550

Granillo-Guerrero, V.G., Villalobos-Espinosa, J.C., Alamilla-Beltrán, L., Téllez-Medina, D.I., Hernández-Sánchez, H., Dorantes-Álvarez, L. and Gutiérrez-López, G.F. (2017). Optimization of the formulation of emulsions prepared with a mixture of vitamins D and E by means of an experimental design simplex centroid and analysis of colocalization of its components. *Revista Mexicana de Ingeniería Química* 16, 816-872. http://rmiq.org/ojs311/index.php/rmiq/article/view/967

Hernández-Carrión, M., Hernando, I., Sotelo-Díaz, I., Quintanilla-Carvajal, M. X. and Quiles, A. (2015). Use of image analysis to evaluate the effect of high hydrostatic pressure and pasteurization as preservation treatments on the microstructure of red sweet pepper. *Innovative Food Science and Emerging Technologies 27* , 69-78. https://doi.org/10.1016/j.ifset.2014.10.011

Hu, X., Zhao, M., Sun, W., Zhao, G. and Ren, J. (2011). Effects of microfluidization treatment and transglutaminase cross-linking on physicochemical, functional, and conformational properties of peanut protein isolate. *Journal of Agricultural and Food Chemistry 59*(16), 8886-8894. https://doi.org/10.1021/jf201781z

Iordache, M. and Jelen, P. (2003). High pressure microfluidization treatment of heat denatured whey proteins for improved functionality. *Innovation Food Science and Emerging Technologies* 4, 367-376. https://doi.org/10.1016/S1466-8564(03)00061-4

Ipsen, R. (2017). Microparticulated whey proteins for improving dairy product texture *International Dairy Journal* 67, 73-79. https://doi.org/10.1016/j.idairyj.2016.08.009

Kang, W., Xu, B., Wang, Y., Li, Y., Shan, X., An, F. and Liu, J. (2011). Stability mechanism of W/O crude oil emulsion stabilized by polymer and surfactant. *Colloids and Surfaces A: Physicochemical and Engineering Aspects* 384, 555-560. https://doi.org/10.1016/j.colsurfa.2011.05.017

Kasaai, M. R., Charlet, G., Paquin, P. and Arul, J. (2003). Fragmentation of chitosan by microfluidization process. *Innovative Food Science & Emerging Technologies*4(4),

403-413. https://doi.org/10.1016/S1466-8564(03)00047-X

Keerati-U-Rai, Maneephan and Corredig, M. (2009). Effect of dynamic high pressure homogenization on the aggregation state of soy protein. *Journal of Agricultural and Food Chemistry* 57(9), 3556-62. https://doi.org/10.1021/jf803562q

Laddi, A., Sharma, S., Kumar, A. and Kapur, P. (2013). Classification of tea grains based upon image texture feature analysis under different illumination conditions. *Journal of Food Engineering.* 115(2), 226-231. https://doi.org/10.1016/j.jfoodeng.2012.10.018

Laneuville, S. I., Paquin, P. and Turgeon, S. L. (2000). Effect of preparation conditions on the characteristics of whey protein-xanthan gum complexes. *Food Hydrocolloids* 14(4), 305-14. https://doi.org/10.1016/S0268-005X(00)00003-5

Li, T., Wang., L., Zhang, X., Geng, H., Xue, W. and Chen, Z. (2020). Assembly behavior, structural characterization and rheological properties of legume proteins based amyloid fibrils. *Food Hydrocolloids* 111, 106396. https://doi.org/10.1016/j.foodhyd.2020.106396

Li, Y.-T., Chen, M.-S., Deng, L.-Z., Liang, Y.-Z., Liu, Y.-K., Liu, W., Chen, J. and Liu, C.-M., (2020).Whole soybean milk produced by a novel industry-scale micofluidizer system without soaking and filtering. *Journal of Food Engineering* 291, 110228. https://doi.org/10.1016/j.jfoodeng.2020.110228

Lin, L., Perets, A., Har-el, Y.E., Varma, D., Li, M., Lazarovici, P., Woerdeman, D.L. and Lelkes, P.I. (2013). Alimentary 'green' proteins as electrospun scaffolds for skin regenerative engineering. *Journal of Tissue Engineering and Regenerative Medicine* 7(12), 994-1008. doi: https://doi.org/10.1002/term.1493

Liu, C.-M., Zhong, J.-Z., Liu, W., Tu, Z.-C., Wan, J., Cai, X.-F. and Song, X.-Y. (2011). Relationship between functional properties and aggregation changes of whey protein induced by high pressure microfluidization. *Journal of Food Science*, *76* (4), E341-E347. https://doi.org/10.1111/j.1750-3841.2011.02134.x

Liu, F. and Tang, C. (2013). Soy protein nanoparticle aggregates as pickering stabilizers for oil-in-water emulsions. *Journal of Agricultural and Food Chemistry* 61 (37) 8888-8898. https://doi.org/10.1021/jf401859y

Liu, F. and Tang, C. (2016) Soy glycinin as food-grade pickering stabilizers: part. II. improvement of emulsification and interfacial adsorption by electrostatic screening. *Food Hydrocolloids* 60, 620-30. https://doi.org/10.1021/jf401859y

Liu, H. H. and Kuo, M.-I. (2016). Ultra high pressure homogenization effect on the proteins in soy flour. *Food Hydrocolloids,* 52, 741-748. https://doi.org/0.1016/j.foodhyd.2015.08.018

Liu, W., Zhang, Z. Q., Liu, C. M., Xie, M. Y., Tu, Z. C., Liu, J. H. and Liang, R. H. (2010). The effect of dynamic high-pressure microfluidization on the activity, stability, and conformation of trypsin. *Food Chemistry* 123 (3), 616-621. https://doi.org/10.1016/j.foodchem.2010.04.079

Madadlou, A., Juliane F., Stephane P. and Didier, D. (2018). Encapsulation of β-lactoglobulin within calcium carbonate microparticles and subsequent *in situ* fabrication of protein microparticles. *Food Hydrocolloids* 84, 38-46. https://doi.org/10.1016/S0268-005X(00)00003-5

Malvern Panalytical (2021). Dynamic light scattering (DLS). Available at: https://www.malvernpanalytical.com/en/products/technology/light-scattering/dynamic-light-scattering.Accessed:January25, 2021.

Martínez, K. D., Vykundeshwari G., Pilosof A. M.R. and Harte, F. M. (2011). Effect of dynamic high-pressure treatment on the interfacial and foaming properties of soy protein isolateehydroxypropylmethylcelluloses systems. *Food Hydrocolloids* 25, 1640-1645.https://doi.org/10.1016/j.foodhyd.2011.02.013

Monroy-Rodríguez I., Monroy-Villagrana A., Cornejo-Mazón M., García-Pinilla S., Hernández-Sánchez H. and Gutiérrez-López G.F. (2020) Microfluidization in nano-food

engineering. *In: Nano-food Engineering*, (Hebbar U., Ranjan S., Dasgupta N., Kumar Mishra R. eds). Pp 153-176. *Food Engineering Series*. Springer, Cham. https://doi.org/10.1007/978-3-030-44552-2_6

Monroy-Villagrana, A., Cano-Sarmiento, C., Alamilla-Beltrán, L., Hernández-Sánchez, H. and Gutiérrez-López, G. (2014). Coupled taguchi-RSM optimization of the conditions to emulsify a-tocopherol in an arabic gum-maltodextrin matrix by microfluidization. *Revista Mexicana de Ingeniería Química*, 13(3), 1-10. http://rmiq.org/iqfvp/Pdfs/Vol.%2013,%20No.%203/Alim3/RMIQTemplate.pdf

Oboroceanu, D., Wang, L., Kroes-Nijboer, A., Brodkorb, A., Venema, P., Magner, E. and Auty, M. A. E. (2011). The effect of high pressure microfluidization on the structure and length distribution of whey protein fibrils. *International Dairy Journal* 21(10), 823-30. https://doi.org/10.1016/j.idairyj.2011.03.015

Ou, X., Pan, W. and Xiao, P. (2014). *In vivo* skin capacitive imaging analysis by using grey level co-occurrence matrix (GLCM). *International Journal of Pharmaceutics* 460(1-2), 28-32. https://doi.org/10.1016/j.ijpharm.2013.10.024

Peles, Z., Binderman, I., Berdicevsky, I. and Zilberman, M. (2012). Soy protein films for wound-healing applications: antibiotic release, bacterial inhibition and cellular response. *Journal of Tissue Engineering and Regenerative Medicine* 7(5),401-12. https://doi.org/10.1002/term.536.

Pereyra-Castro, S., Pérez-Pérez, V., Hernández-Sánchez, H., Jiménez-Aparicio, A., Gutiérrez-López, G. and Alamilla-Beltrán, L. (2019). Effect of composition and homogenization pressure of chia oil emulsions elaborated by microfluidization. *Revista Mexicana De Ingeniería Química* 18(1), 69-81. https://doi.org/10.24275/uam/izt/dcbi/revmexingquim/2019v18n1/Pereyra

Qi. X., Dond, Y., Wang, H., Wang C. and Li, F. (2017). Application of Turbiscan in the homoaggregation and heteroaggregation of copper nanoparticles. *Colloids and Surfaces A* 535, 96-104. DOI: https://doi.org/10.1016/j.colsurfa.2017.09.015

Qiao, J., Ngadi, M. O., Wang, N., Gariépy, C. and Prasher, S. O. (2007). Pork quality and marbling level assessment using a hyperspectral imaging system. *Journal of Food Engineering* 83(1), 10-16. https://doi.org/10.1016/j.jfoodeng.2007.02.038

Quintanilla-Carvajal, M. X., Meraz-Torres, L. S., Alamilla-Beltrán, L., Chanona-Pérez, J. J.,Terres-Rojas, E., Hernández-Sánchez, H., Jimenez-Aparicio, A.R. and Gutierrez-López G.F. (2011). Morphometric characterization of spray-dried microcapsules before and after a-tocopherol extraction. *Revista Mexicana de Ingenieria Química* 10, 301-312. http://www.rmiq.org/ojs311/index.php/rmiq/article/view/1674

Shen, L. and Tang, C. H. (2012). Microfluidization as a potential technique to modify surface properties of soy protein isolate. *Food Research International* 48(1), 108-118. https://doi.org/10.1016/j.foodres.2012.03.006

Sivchenko, N., Kvaal, K. and Ratnaweera., H. (2016). Evaluation of image texture recognition techniques in application to wastewater coagulation. *Cogent Engineering* 3, 1206679. https://doi.org/10.1080/23311916.2016.1206679

Song, X., Chengjun Z., Feng F., Zhilin C. and Qinglin W. (2013). Effect of high-pressure homogenization on particle size and film properties of soy protein isolate. *Industrial Crops and Products* 43(1), 538-44. https://doi.org/10.1016/j.indcrop.2012.08.005

Sun, C., Lei D., Fuguo L. and Yanxiang G. (2016) Dynamic high pressure microfluidization treatment of zein in aqueous ethanol solution. *Food Chemistry* 210, 388-95. https://doi.org/10.1016/j.foodchem.2016.04.138

Tang, C.-H., Xiao, Y.-W., Xiao, Q.-Y. and Lin, L. (2009). Formation of soluble aggregates from insoluble commercial soy protein isolate by means of ultrasonic treatment and their gelling properties. *Journal of Food Engineering*

92(4), 432-37. https://doi.org/10.1016/j.jfoodeng.2008.12.017

Tang C.H. and Liu F. (2013) Cold, gel-like soy protein emulsions by microfluidization: Emulsion characteristics, rheological and microstructural properties, and gelling mechanism. *Food Hydrocolloids,* 30(1), 61-72. https://doi.org/10.1016/j.foodhyd.2012.05.008

Torres, I. C., Janhoj, T., Mikkelsen, B.O. and Ipsen, R. (2011). Effect of microparticulated whey protein with varying content of denatured protein on the rheological and sensory characteristics of low-fat yoghurt. *International Dairy Journal* 21, 645-655. https://doi.org/10.1016/j.idairyj.2010.12.013

Villalobos-Castillejos, F., Granillo-Guerrero, V. G. and Diana, E. Alamilla-Beltrán L., Gutiérrez-López, G. F., Monroy-Villagrana, A. and Jafari, S.M. (2018). Fabrication of nanoemulsions by microfluidization. In: *Nanoemulsions formulation, applications, and characterization* (Seid Mahdi Jafari, David Julian McClements, eds). Pp 207-232. Academic Press. https://doi.org/10.1016/B978-0-12-811838-2.00008-4.

Villalobos-Espinosa, J., Quintanilla-Carvajal, M., Granillo-Guerrero, V., Alamilla-Beltrán, L., Hernández-Sánchez, H., Perea-Flores, M., Azura-Nieto, E. and Gutiérrez-López, G. (2019). Effect of two-fluid nozzles on the stability characteristics of emulsions prepared by a high-energy method (microfluidization).*Revista Mexicana de Ingeniería Química18*(1), 165-80. https://doi.org/10.24275/uam/izt/dcbi/revmexingquim/2019v18n1/Villalobos

Wen, Y., Xu, Z., Liu, Y., Corke, H. and Sui, Z. (2020). Investigation of food microstructure and texture using atomic force microscopy: A review. *Comprehensive Reviews in Food Science and Food Safety 19*(5), 2357-2379. https://doi.org/10.1111/1541-4337.12605

Yang, X., Beyenal, H., Harkin, G. and Lewandowski, Z. (2000). Quantifying biofilm structure using image analysis. *Journal of Microbiological Methods* 39(2), 109-119. https://doi.org/10.1016/s0167-7012(99)00097-4

Zhong, J. Z., Liu, W., Liu, C. M., Wang, Q. H., Li, T., Tu, Z. C., Cai, X.C. and Xu, Y. J. (2012). Aggregation and conformational changes of bovine β-lactoglobulin subjected to dynamic high-pressure microfluidization in relation to antigenicity. *Journal of Dairy Science 95*(8), 4237-4245. https://doi.org/10.3168/jds.2012-5333